

AD-A266 748



MENTATION PAGE

Form Approved  
OMB No. 0704-0188

estimated to average 1 hour per response, including the time for reviewing instructions, searching existing data sources, and reviewing the collection of information. Send comments regarding this burden estimate or any other aspect of this burden to Washington Headquarters Services, Directorate for Information Operations and Reports, 1215 Jefferson to the Office of Management and Budget, Paperwork Reduction Project (0704-0188), Washington, DC 20503

REPORT DATE  
PRIL 15, 1993

3. REPORT TYPE AND DATES COVERED  
Final 15 Sep 89 - 14 Mar 93

25

4. TITLE AND SUBTITLE  
Turbulence and Transition Modeling  
for High-Speed Flows

5. FUNDING NUMBERS

6. AUTHOR(S)  
David C. Wilcox

DTIC  
S ELECTE D  
JUL 09 1993  
A

7. PERFORMING ORGANIZATION NAME(S) AND ADDRESS(ES)  
DCW Industries, Inc.  
5354 Palm Drive  
La Canada, California 91011

8. PERFORMING ORGANIZATION  
REPORT NUMBER  
392052  
93-15481  
10pp

9. SPONSORING/MONITORING AGENCY NAME(S) AND ADDRESS(ES)  
U. S. Army Research Office  
P. O. Box 12211  
Research Triangle Park, NC 27709-2211

ARO 26863.8-EGS

11. SUPPLEMENTARY NOTES  
The view, opinions and/or findings contained in this report are those of the author(s) and should not be construed as an official Department of the Army position, policy, or decision, unless so designated by other documentation.

12a. DISTRIBUTION/AVAILABILITY STATEMENT  
Approved for public release; distribution unlimited.

12b. DISTRIBUTION CODE

93 7 08 052

13. ABSTRACT (Maximum 200 words)  
This report summarizes research conducted during the past three and a half years aimed at developing and testing a turbulence/transition model applicable to high-speed turbulent flows. The first two years of the project focused on fully turbulent flows, while emphasis shifted to boundary-layer development in the transition region during the final year and a half. This report includes a brief summary of research accomplished during the first three years and cites publications that describe research results in greater detail. The main body of this report summarizes research conducted during the final six months of the period of performance. The primary results of the last six months of the project are elimination of the k-w model's sensitivity to the freestream value of w and development of a method for triggering transition at a specified location, independent of the freestream turbulence level.

14. SUBJECT TERMS  
TRANSITION, TURBULENCE MODELING, HYPERSONICS,  
COMPUTATIONAL FLUID DYNAMICS

15. NUMBER OF PAGES  
38

16. PRICE CODE

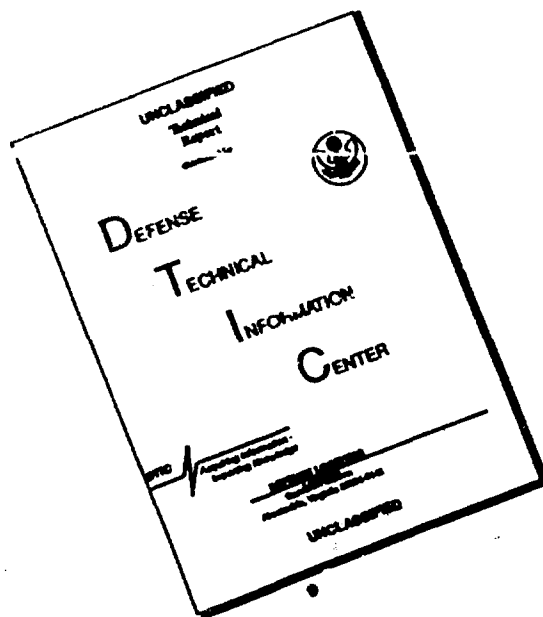
17. SECURITY CLASSIFICATION  
OF REPORT  
UNCLASSIFIED

18. SECURITY CLASSIFICATION  
OF THIS PAGE  
UNCLASSIFIED

19. SECURITY CLASSIFICATION  
OF ABSTRACT  
UNCLASSIFIED

20. LIMITATION OF ABSTRACT  
UL

# DISCLAIMER NOTICE



**THIS DOCUMENT IS BEST QUALITY AVAILABLE. THE COPY FURNISHED TO DTIC CONTAINED A SIGNIFICANT NUMBER OF PAGES WHICH DO NOT REPRODUCE LEGIBLY.**

# Contents

<b>1 Introduction</b>	<b>2</b>
<b>2 Revised Low Reynolds Number <math>k-\omega</math> Model</b>	<b>5</b>
<b>3 Turbulent Boundary-Layer Applications</b>	<b>8</b>
<b>4 Free Shear Flow Applications</b>	<b>15</b>
<b>5 Transitional Boundary-Layer Applications</b>	<b>18</b>
5.1 Triggering Transition . . . . .	18
5.2 Applications . . . . .	19
<b>6 Summary and Conclusions</b>	<b>29</b>
<b>A Compressible Law of the Wall</b>	<b>30</b>
<b>References</b>	<b>36</b>

DTIC QUALITY INSPECTED 8

Accession For	
NTIS CRA&I	<input checked="" type="checkbox"/>
DTIC TAB	<input type="checkbox"/>
Unannounced	<input type="checkbox"/>
Justification	
By	
Distribution/	
Availability Codes	
Dist	Avail and/or Special
A-1	

# Abstract

This report summarizes research conducted during the past three and a half years aimed at developing and testing a turbulence/transition model applicable to high-speed turbulent flows. The first two years of the project focused on fully turbulent flows, while emphasis shifted to boundary-layer development in the transition region during the final year and a half. This report includes a brief summary of research accomplished during the first three years and cites publications that describe research results in greater detail. The main body of this report summarizes research conducted during the final six months of the period of performance. The primary results of the last six months of the project are elimination of the  $k-\omega$  model's sensitivity to the freestream value of  $\omega$  and development of a method for triggering transition at a specified location, independent of the freestream turbulence level.

# Chapter 1

## Introduction

The purpose of this research project for the past three and a half years has been to develop analytical and computational tools suitable for predicting properties of hypersonic flows, including both turbulent and transitional flow regimes. Our research efforts have generated a total of eight publications, including this final report. The previous publications are as follows.

1. Wilcox, D. C., "Hypersonic Turbulence Modeling Without the Epsilon Equation," 7<sup>th</sup> National Aero-Space Plane Technology Symposium, Session VII, Paper No. 27 (October 1989).
2. Wilcox, D. C., "A Half Century Historical Review of the  $k-\omega$  Model," AIAA Paper 91-0615 (January 1991).
3. Wilcox, D. C., "Theoretical Study of Turbulent Mixing Between Hypersonic Streams," DCW Industries Report No. DCW-R-35-01 (May 1991).
4. Wilcox, D. C., "Progress in Hypersonic Turbulence Modeling," AIAA Paper 91-1785 (June 1991).
5. Wilcox, D. C., "Progress in Developing a Transition Model for High-Speed Flows," DCW Industries Report No. DCW-R-35-02 (October 1992).
6. Wilcox, D. C., "The Remarkable Ability of Turbulence Model Equations to Describe Transition," *Fifth Symposium on Numerical and Physical Aspects of Aerodynamic Flows*, California State University, Long Beach, California (13-15 January 1992) [accepted for publication in the AIAA Journal].
7. Wilcox, D. C., "Dilatation-Dissipation Corrections for Advanced Turbulence Models," *AIAA Journal*, Vol. 30, No. 11, pp. 2639-2646 (November 1992).

Publications 1, 3, 4 and 7 deal primarily with fully-turbulent, high-speed flows, and represent research results for the first two years of the project. One of the primary accomplishments was discovery that separating dissipation into solenoidal and dilatation contributions improves predictive accuracy for the compressible mixing layer at the expense of a loss in predictive accuracy for boundary layers. We identified the cause of this problem and postulated a dilatation-dissipation correction that is accurate for the mixing layer and the boundary layer. A second accomplishment was identification that the  $k-\omega$  model faithfully reproduces the compressible law of the wall for high-speed flows while the  $k-\epsilon$  model does not. Perhaps the most important accomplishment was the demonstration, in Publications 4 and 7 that dilatation dissipation does little to improve two-equation-model predictions for shock-separated flows. Rather, the research verifies that using a second-order closure model greatly improves predicted size of the separation region, although other flow properties are not accurately predicted (e.g., velocity profiles downstream of the reattachment point).

Publications 2, 4 and 6 introduce low-Reynolds-number corrections for the  $k-\omega$  model that permit the model to accurately describe near-wall properties of high-speed boundary layers. The modifications presented in the first two publications ultimately have been superseded by those postulated in Publication 6. The latter Publication represents much of the basic research conducted during the third year of the project.

Publications 5 and 6 focus on application of the low-Reynolds-number  $k-\omega$  model to a collection of transitional flows. The publications show that the model accurately predicts properties in the transitional region provided transition Reynolds number is relatively small. By contrast, predicted transition width is generally smaller than measured for transition at high Reynolds numbers. Additionally, computed results show a stronger-than-desired sensitivity to the freestream value of  $\omega$ , and the need for a simple method of triggering transition at a specified location.

During the final six months of the project, we have eliminated two of the three outstanding problems with the model as it applies to transitional boundary layers. Specifically, we have devised a modification that eliminates solution sensitivity to the freestream value of  $\omega$ , and we have devised a straightforward method for triggering transition at a specified location. However, limited funding has precluded solving the problem of the too-abrupt transition at high Reynolds numbers.

As summarized in Publication 5, the overall objective of our approach to the transition problem is to use the Wilcox<sup>1</sup>  $k-\omega$  turbulence model as the foundation for studying and modeling the transitional flow region. Consistent with the needs of NASA, the transition point is assumed to be known a priori. Computations can thus be initiated at the known transition location and continued downstream through the transitional flow region and well into the fully turbulent region. To develop the model, we have followed a sequence of interrelated steps.

1. In Publications 2, 4 and 6, we drew from the extensive work done by Wilcox et al.<sup>2-7</sup> to help formulate a low-Reynolds-number version of the  $k-\omega$  model.
2. In Publications 4 and 6, we simulated several of the flows that have been done with Direct Numerical Simulation (DNS) methods. The results of Mansour, Kim and Moin<sup>8</sup> were computed for two different Reynolds numbers. Comparing model predictions with the DNS results helped greatly in developing the model.
3. In Publication 5, we tested the model against 10 two-dimensional, fully turbulent boundary layers, including both incompressible and compressible cases. We have repeated 5 of these cases in this report.
4. In Publication 5, we tested the model against all of the two-dimensional cases presented by Singer, Dinavahi, and Iyer.<sup>9</sup> We have repeated all of these cases in this report.
5. We have analyzed the compressible log layer to explain why adding a cross-diffusion term to the  $\omega$  equation can have an adverse effect on predicted skin friction.

As noted above, addressing Items 1 and 2 has produced a low-Reynolds-number version of the  $k-\omega$  model. Publication 6 describes the model and presents applications to fully turbulent channel and pipe flow, and for a transitional, incompressible flat-plate boundary layer. In this report we propose a modified version of the model that eliminates freestream boundary-condition sensitivity. This report applies the model to 5 turbulent boundary-layer test cases, two free shear flow cases and to more than 20 transitional flows for which experimental data are available.

Chapter 2 summarizes the revised low-Reynolds-number version of the  $k-\omega$  model. Chapters 3, 4 and 5 present results of our applications. Chapter 6 summarizes results of the research. The effect of a model revision on the compressible law of the wall is discussed in Appendix A.

## Chapter 2

# Revised Low Reynolds Number $k-\omega$ Model

The revised low-Reynolds-number version of the  $k-\omega$  model is written in terms of Favre<sup>10</sup> mass averaged variables. The equations of motion are as follows.

$$\frac{\partial \rho}{\partial t} + \frac{\partial}{\partial x_j} (\rho u_j) = 0 \quad (2.1)$$

$$\frac{\partial}{\partial t} (\rho u_i) + \frac{\partial}{\partial x_j} (\rho u_j u_i) = -\frac{\partial p}{\partial x_i} + \frac{\partial \tau_{ji}}{\partial x_j} \quad (2.2)$$

$$\frac{\partial}{\partial t} (\rho E) + \frac{\partial}{\partial x_j} (\rho u_j H) = \frac{\partial}{\partial x_j} \left[ u_i \tau_{ij} - q_j + (\mu + \sigma^* \mu_T) \frac{\partial k}{\partial x_j} \right] \quad (2.3)$$

$$\frac{\partial}{\partial t} (\rho k) + \frac{\partial}{\partial x_j} (\rho u_j k) = \tau_{ij}^T \frac{\partial u_i}{\partial x_j} - \beta^* \rho \omega k + \frac{\partial}{\partial x_j} \left[ (\mu + \sigma^* \mu_T) \frac{\partial k}{\partial x_j} \right] \quad (2.4)$$

$$\begin{aligned} \frac{\partial}{\partial t} (\rho \omega) + \frac{\partial}{\partial x_j} (\rho u_j \omega) &= \alpha \frac{\omega}{k} \tau_{ij}^T \frac{\partial u_i}{\partial x_j} - \beta \rho \omega^2 + \sigma_d \frac{\rho}{\omega} \frac{\partial k}{\partial x_j} \frac{\partial \omega}{\partial x_j} \\ &+ \frac{\partial}{\partial x_j} \left[ (\mu + \sigma \mu_T) \frac{\partial \omega}{\partial x_j} \right] \end{aligned} \quad (2.5)$$

In Equations (2.1)-(2.5),  $t$  and  $x_i$  denote time and position vector;  $\rho$  and  $p$  are density and pressure;  $u_i$  is mass-averaged velocity vector;  $E$  and  $H$  are total energy and total enthalpy;  $\tau_{ij}$  and  $q_i$  are the total stress tensor and the total heat flux vector;  $\tau_{ij}^T$  is the Reynolds stress tensor;  $k$  and  $\omega$  are turbulence

kinetic energy and specific dissipation rate; and,  $\alpha$ ,  $\beta$ ,  $\beta^*$ ,  $\sigma$ ,  $\sigma^*$ ,  $\sigma_d$  are closure coefficients. The following constitutive relations are needed to close the system.

$$\mu_T = \alpha^* \frac{\rho k}{\omega}, \quad \tau_{ij} = \tau_{ij}^L + \tau_{ij}^T \quad (2.6)$$

$$\tau_{ij}^L = 2\mu \left( S_{ij} - \frac{1}{3} \frac{\partial u_k}{\partial x_k} \delta_{ij} \right) \quad (2.7)$$

$$\tau_{ij}^T = 2\mu_T \left( S_{ij} - \frac{1}{3} \frac{\partial u_k}{\partial x_k} \delta_{ij} \right) - \frac{2}{3} \rho k \delta_{ij} \quad (2.8)$$

$$q_j = - \left( \frac{\mu}{Pr_L} + \frac{\mu_T}{Pr_T} \right) \frac{\partial h}{\partial x_j} \quad (2.9)$$

$$E = e + \frac{1}{2} u_i u_i + k, \quad H = h + \frac{1}{2} u_i u_i + k \quad (2.10)$$

$$S_{ij} = \frac{1}{2} \left( \frac{\partial u_i}{\partial x_j} + \frac{\partial u_j}{\partial x_i} \right) \quad (2.11)$$

In the constitutive relations, we have introduced the molecular stress tensor,  $\tau_{ij}^L$ , mean strain-rate tensor,  $S_{ij}$ , molecular viscosity,  $\mu$ , eddy viscosity,  $\mu_T$ , enthalpy,  $h$ , laminar Prandtl number,  $Pr_L$ , turbulent Prandtl number,  $Pr_T$ , internal energy,  $e$ , and an additional closure coefficient,  $\alpha^*$ . Finally, to complete closure of the system, we specify the values of the closure coefficients as follows.

$$\alpha^* = \frac{\alpha_o^* + Re_T/R_k}{1 + Re_T/R_k}, \quad \alpha = \frac{1}{2} \cdot \frac{\alpha_o + Re_T/R_\omega}{1 + Re_T/R_\omega} \cdot (\alpha^*)^{-1} \quad (2.12)$$

$$\beta^* = \frac{9}{100} \cdot \frac{5/18 + (Re_T/R_\beta)^4}{1 + (Re_T/R_\beta)^4} \quad (2.13)$$

$$\beta = \frac{3}{40}, \quad \sigma^* = 1, \quad \sigma = \frac{3}{5} \quad (2.14)$$

$$\sigma_d = \begin{cases} 0, & \frac{\partial k}{\partial x_j} \frac{\partial \omega}{\partial x_j} \leq 0 \\ \frac{3}{10}, & \frac{\partial k}{\partial x_j} \frac{\partial \omega}{\partial x_j} > 0 \end{cases} \quad (2.15)$$

$$\alpha_o^* = \beta/3, \quad \alpha_o = 1/10 \quad (2.16)$$

$$R_\beta = 6, \quad R_k = 8, \quad R_\omega = 11/5 \quad (2.17)$$

The quantity  $Re_T$  is the turbulence Reynolds number defined by

$$Re_T = \frac{\rho k}{\omega \mu} \quad (2.18)$$

The primary difference between this model and the model introduced by Wilcox<sup>11</sup> is the introduction of the term in Equation (2.5) proportional to  $\sigma_d$ . This term is similar to Menter's<sup>12</sup> cross-diffusion term. The effect of this term is to replace the entrainment velocity,  $v$ , in the  $\omega$  equation by  $(v - \sigma_d \omega^{-1} \partial k / \partial y)$ . Since  $k$  decreases approaching the shear layer edge (assuming  $\sigma_d > 0$ ), the net effect is to make the effective entrainment velocity positive (or at least less negative). As a result,  $\omega$  diffuses from the turbulent region into the nonturbulent region, which is the opposite of what happens with the  $k$ - $\omega$  model. Thus, the freestream value of  $\omega$  has no effect on the solution.

As shown by Wilcox<sup>13</sup>, it is important to suppress the cross-diffusion term close to solid boundaries for wall-bounded flows. The prescription in Equation (2.15) causes  $\sigma_d$  to vanish near a solid boundary since  $k$  increases and  $\omega$  decreases in the viscous sublayer. This modification to the  $\omega$  equation eliminates the model's sensitivity to the freestream value of  $\omega$ . The values of several closure coefficients must be modified to achieve optimum results for both boundary layers and free shear layers. Specifically,  $\sigma$  and  $\sigma^*$  must assume values larger than used in the Standard  $k$ - $\omega$  model. This, in turn, requires changing  $\alpha$  and  $R_\omega$  to maintain a satisfactory law of the wall in the turbulent boundary layer. The value quoted for  $\alpha$  guarantees that the Kármán constant is 0.41 while the value of  $R_\omega$  yields an additive constant in the law of the wall of 5.0. In summary, Table 2.1 shows how the revised model's closure coefficients differ from those of the Wilcox<sup>11</sup> model.

Table 2.1: Closure Coefficient Differences

Coefficient	New Model	Wilcox <sup>11</sup> Model
$\sigma$	3/5	1/2
$\sigma^*$	1	1/2
$\sigma_d$	Equation (2.15)	0
$\alpha$	1/2	5/9
$R_\omega$	11/5	27/10

## Chapter 3

# Turbulent Boundary-Layer Applications

A key objective of research during the final year and a half of this project has been to describe boundary-layer development through transition from laminar to turbulent flow. Of course, it is important that we provide an accurate description in the turbulent region immediately following transition, i.e., we insist that our model approach the proper limiting state of the boundary layer. Consequently, since the  $k-\omega$  model without viscous corrections generally is very accurate for turbulent boundary layers, a round of tests is in order to make sure model predictions are not adversely affected by the viscous corrections. We have performed five boundary layer computations including effects of adverse and favorable pressure gradient, and for Mach numbers as high as 10. Table 3.1 lists the five cases.

Table 3.1: Turbulent Boundary Layer Test Cases

Description	$\nabla p$	Data Source
Incompressible Flat Plate	None	Wieghardt-Tillman <sup>14</sup>
Samuel-Joubert	Adverse	Samuel-Joubert <sup>15</sup>
Mach 2.244 Flat Plate	None	Shutts <sup>16</sup>
Mach 4.544 Flat Plate	None	Coles <sup>16</sup>
Mach 10.31 Flat Plate	None	Watson <sup>16</sup>

**Incompressible Flat Plate.** Figure 3.1 compares computed and measured skin friction,  $c_f$ , and sublayer-scaled velocity,  $u^+$ . As shown, the only significant difference between predictions with and without viscous corrections is in the transition point. The unmodified model undergoes transition much earlier than

the model with viscous corrections. Skin friction at the final station is  $2.51 \cdot 10^{-3}$  with viscous modifications compared to  $2.49 \cdot 10^{-3}$  without.

**Samuel-Joubert.** This incompressible adverse pressure gradient boundary layer was supposed to be a simple application in Stanford Olympics II.<sup>17</sup> On the contrary, it proved to be very difficult for all models and has become a key test case for how well a turbulence model predicts effects of adverse pressure gradient. Figure 3.2 shows that both high- and low-Reynolds-number versions of the model nearly duplicate measured skin friction and velocity profile at the last station. At the final station,  $c_f = 1.35 \cdot 10^{-3}$  with viscous corrections and  $1.25 \cdot 10^{-3}$  without.

**Compressible Flat Plates.** As shown in Figures 3.3, 3.4 and 3.5, the viscous corrections have virtually no effect on skin friction and velocity profiles in the fully turbulent region for these three applications. For all three cases, skin friction differs by less than one percent at the final station.

**In summary,** for all 5 cases considered, differences between computed flow properties with and without viscous corrections are less than 8%, and are generally less than 2%. Additionally, although not shown here, we have computed (under separate funding) 14 more incompressible boundary layers, 3 with favorable pressure gradient and 11 with adverse pressure gradient. Along with the flat-plate boundary layer and the Samuel-Joubert case, these are the 16 boundary layers analyzed by Wilcox<sup>18</sup>. As with the cases discussed above, the low-Reynolds-number  $k-\omega$  model is as accurate as the basic model without viscous modifications. Hence, the viscous corrections leave the best features of the  $k-\omega$  model intact, i.e., the model still accurately predicts effects of pressure gradient and compressibility up to Mach 5.

While the cross-diffusion term in the  $\omega$  equation greatly reduces the model's sensitivity to the freestream value of  $\omega$ , it does not entirely remove it. A larger value of  $\sigma_d$  is needed to completely remove the sensitivity. However, as shown in Appendix A, using a larger value for  $\sigma_d$  yields an inaccurate prediction for the compressible law of the wall.

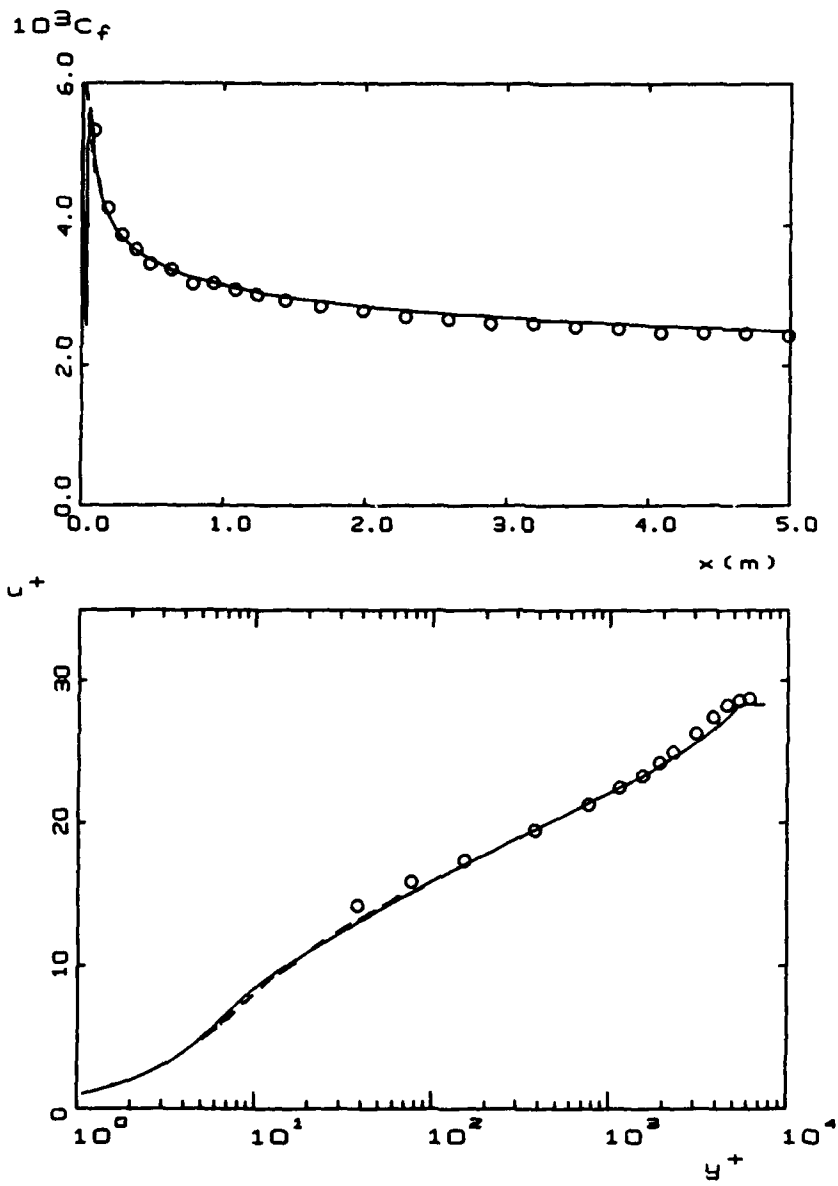


Figure 3.1: Incompressible flat-plate boundary layer;  $\circ$  Wieghardt-Tillman; —  $k-\omega$  with viscous corrections; - -  $k-\omega$  without viscous corrections.

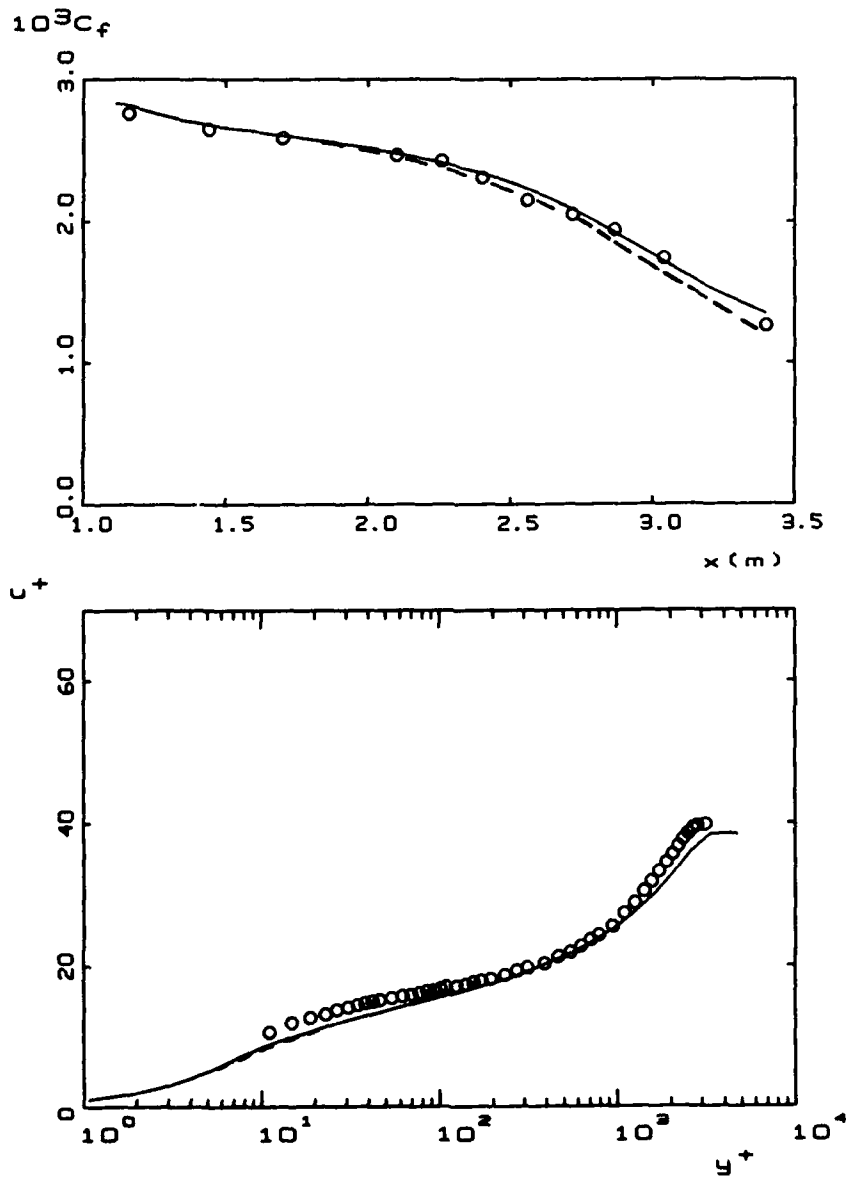


Figure 3.2: Incompressible boundary layer in an increasingly adverse pressure gradient;  $\circ$  Samuel-Joubert; —  $k-\omega$  with viscous corrections; - -  $k-\omega$  without viscous corrections.

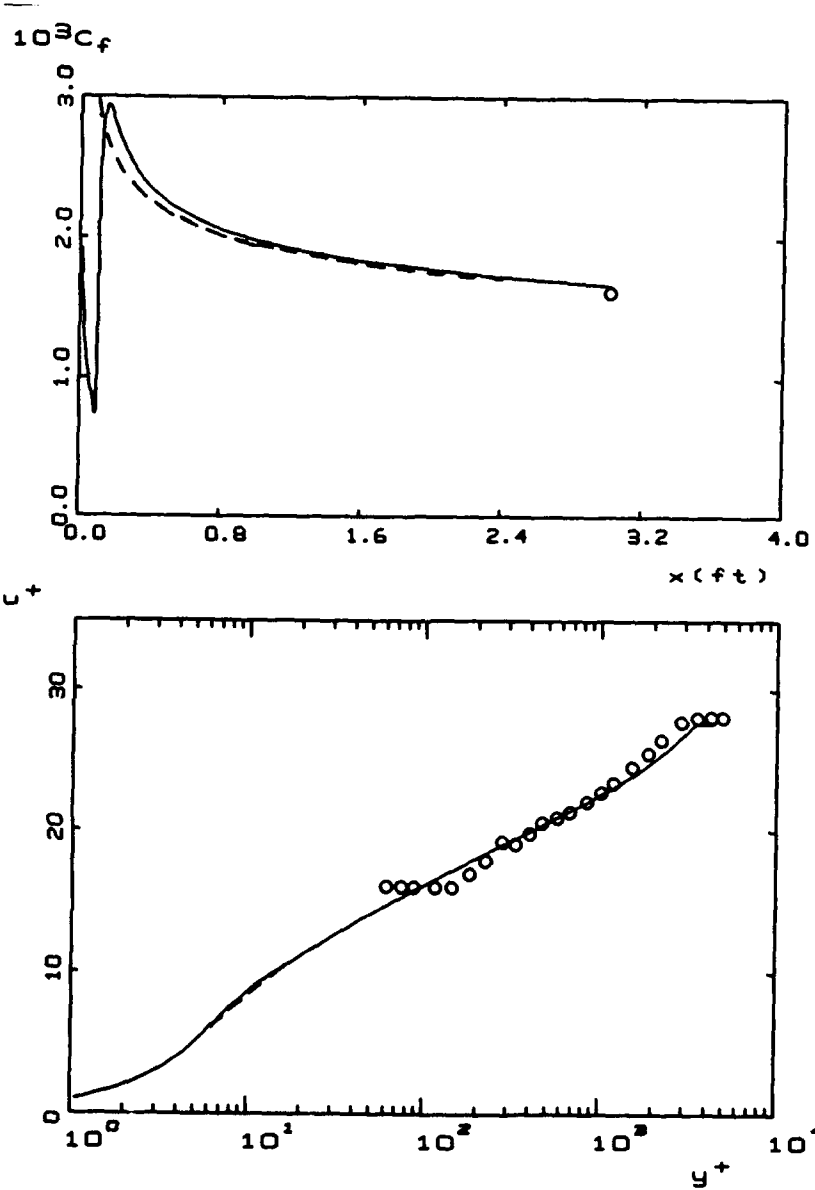


Figure 3.3: Mach 2.244 adiabatic-wall flat-plate boundary layer;  $\circ$  Shutts; —  $k-\omega$  with viscous corrections; - - -  $k-\omega$  without viscous corrections.

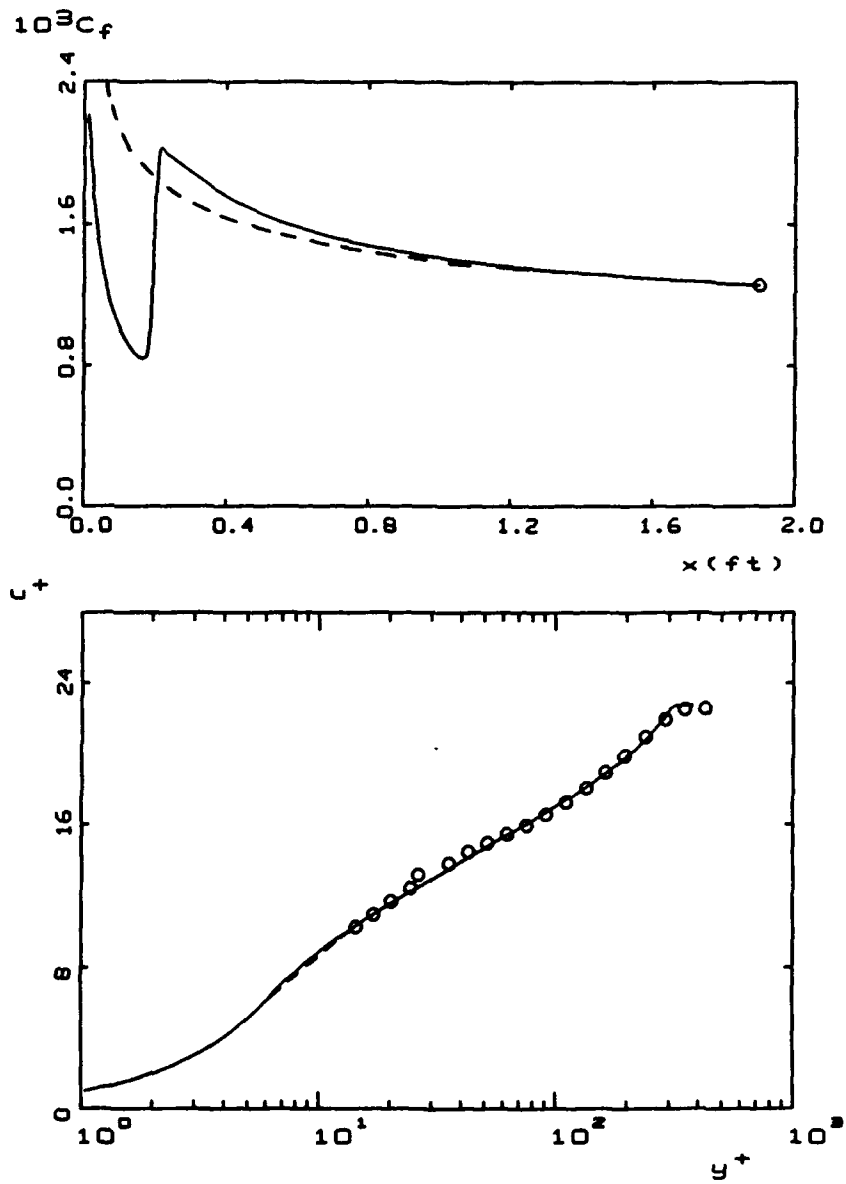


Figure 3.4: Mach 4.544 adiabatic-wall flat-plate boundary layer;  $\circ$  Coles; —  $k-\omega$  with viscous corrections; - - -  $k-\omega$  without viscous corrections.

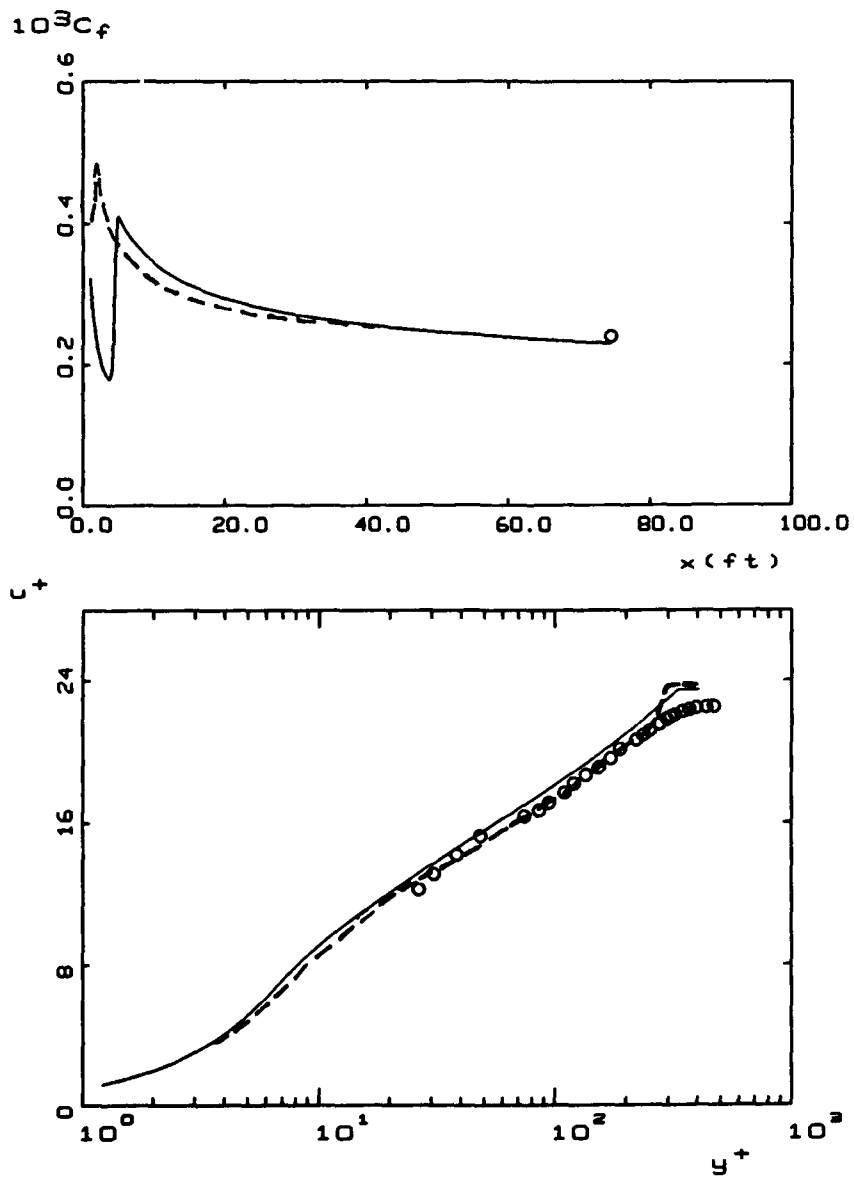


Figure 3.5: Mach 10.31 adiabatic-wall flat-plate boundary layer;  $\circ$  Watson; —  $k-\omega$  with viscous corrections; - -  $k-\omega$  without viscous corrections.

## Chapter 4

# Free Shear Flow Applications

While  $k-\omega$  model boundary-layer computations display a mild sensitivity to the freestream value of  $\omega$ , the sensitivity is much stronger for free shear flows. As shown by Wilcox<sup>13</sup>, the spreading rate for the incompressible mixing layer varies between 0.103 and 0.141; the measured spreading rate is 0.115. Similarly, for the far wake, computed spreading rate varies from 0.301 to 0.500, as compared to a measured value of 0.365.

The new model almost completely eliminates this problem. Figure 4.1 compares computed and measured mixing-layer velocity profiles for two values of the freestream  $\omega$  that differ by several orders of magnitude. The computed spreading rate varies between 0.105 and 0.107.

Similarly, Figure 4.2 compares computed and measured velocity profiles for the far wake. For a wide range of freestream values of  $\omega$ , the spreading rate varies between 0.295 and 0.318.

We have attempted computations for the plane and round jets, but have encountered numerical difficulties in obtaining converged solutions. This illustrates a key problem attending use of the cross-diffusion term. In general, the term greatly increases the stiffness of the model equations by altering the effective time scale ( $\omega^{-1}$ ) near a turbulent/nonturbulent interface. As a consequence, the convergence rate of the numerical algorithm tends to be reduced.

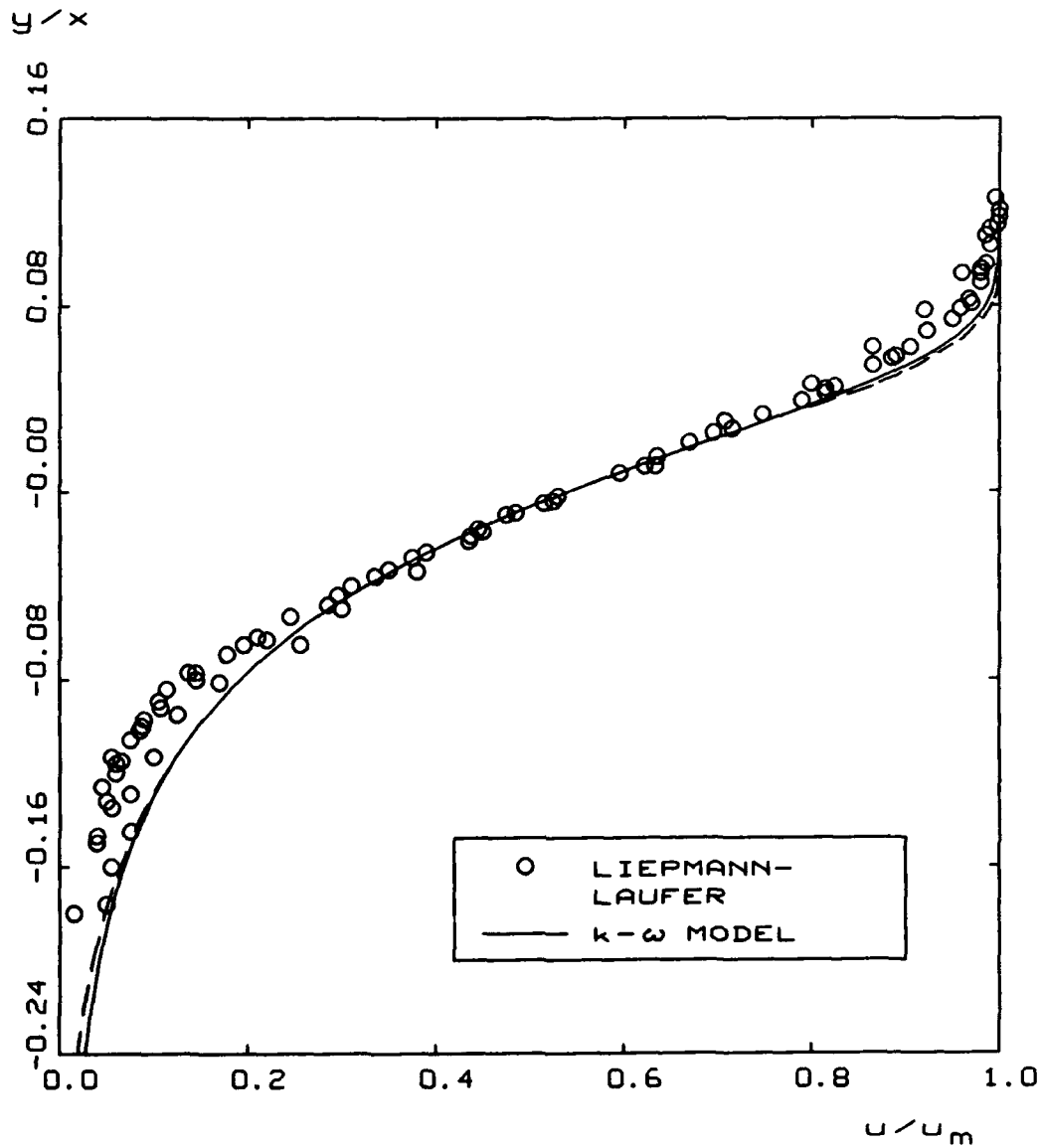


Figure 4.1: Comparison of computed and measured incompressible mixing-layer velocity profiles;  $\circ$  Liepmann-Laufer; —  $\omega_\infty \rightarrow 0$ ; - - -  $\omega_\infty$  finite.

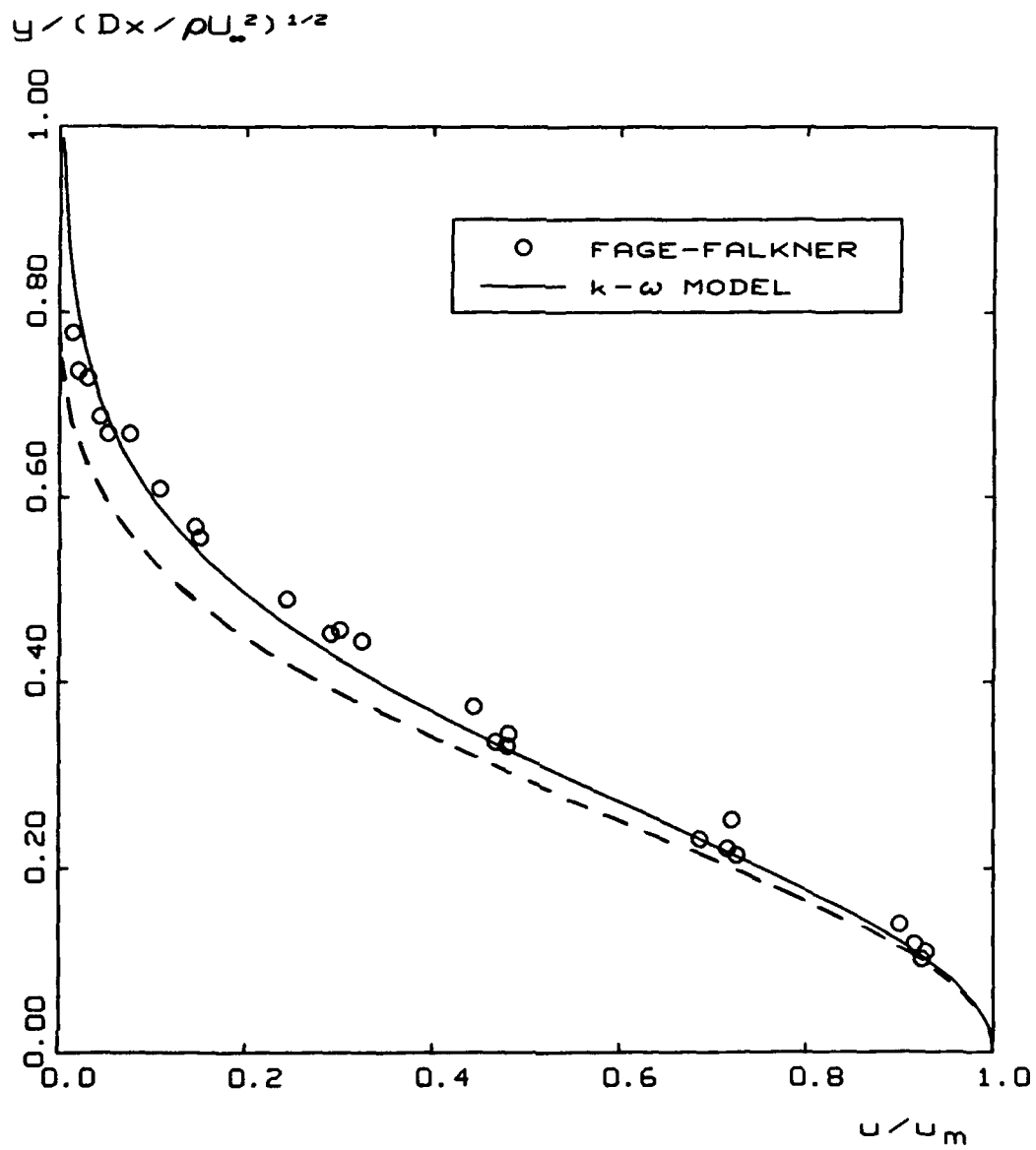


Figure 4.2: Comparison of computed and measured incompressible far-wake velocity profiles; ○ Fage-Falkner; —  $\omega_\infty \rightarrow 0$ ; - - -  $\omega_\infty$  finite.

## Chapter 5

# Transitional Boundary-Layer Applications

### 5.1 Triggering Transition

The question of how to trigger transition for a given application raises an important point about using turbulence-model equations for transitional flows. We must keep in mind that transition is a complicated phenomenon. Transition is triggered by a disturbance in a boundary layer only if the frequency of the disturbance falls in a specific band. Reynolds averaging has masked all spectral effects, and all the model can represent with  $k$  and  $\omega$  is the intensity of the disturbance and an average frequency. Hence, it is possible for the turbulence model to predict transition when it shouldn't occur. If we choose to trigger transition via the presence of a freestream disturbance, using turbulence-model equations is sensible only if the triggering disturbance is broad band, i.e., contains all frequencies.

In devising the model, the closure coefficients  $\alpha_0^*$  and  $\alpha_0$  [Equation (2.16)] have been chosen to match the minimum critical Reynolds number for the Blasius boundary layer. Consequently, the model can be expected to yield sensible transition predictions for constant-pressure, incompressible boundary layers. Unfortunately, the model equations must be recalibrated (i.e.,  $\alpha_0^*$  and  $\alpha_0$  must be adjusted) to accommodate each new complicating effect [see Wilcox et al.<sup>2-7</sup>].

In this project, the goal has been to assume the transition point is given and to use the model equations through the transitional region and into the turbulent part of the flow. To date, the freestream turbulence intensity, proportional to the freestream value of  $k$ , has been adjusted to match the measured transition

point. This is satisfactory when the transition point occurs at a large Reynolds number, which requires  $k_\infty$  to be small relative to  $U_\infty^2$ . However, for high-speed flows in which transition occurs at a relatively small Reynolds number, we have found that unreasonably large values of  $k_\infty$  are needed to trigger transition, so large as to affect the total energy in the freestream in a physically unrealistic manner. Thus, a new method for triggering transition is needed.

To devise an alternative method, we can take advantage of a unique feature of the  $k$ - $\omega$  model. Specifically, by using a finite value for  $\omega$  at the surface, we can simulate surface roughness with the model. For fully turbulent boundary layers, Wilcox<sup>1</sup> shows that

$$\omega = \frac{u_\tau^2}{\nu} S_R \quad \text{at} \quad y = 0 \quad (5.1)$$

where  $u_\tau$  is friction velocity and  $S_R$  is a dimensionless function of the surface roughness height,  $k_R$ , defined by (with  $k_R^+ = u_\tau k_R / \nu$ ):

$$S_R = \begin{cases} (50/k_R^+)^2, & k_R^+ < 25 \\ 100/k_R^+, & k_R^+ \geq 25 \end{cases} \quad (5.2)$$

Since increasing the surface roughness height corresponds to decreasing the surface value of  $\omega$  (and thus the dissipation in the  $k$  equation), the model predicts that roughness will have a destabilizing effect. This is consistent with measurements, and patches of surface roughness are often used to trigger transition in experiments. Thus, a possible way to trigger transition with the model equations is to numerically simulate a roughness strip via Equations (5.1) and (5.2).

We have run more than 20 two-dimensional transitional boundary layer cases to test this idea; results of the computations are given in the next section. We have been able to trigger transition at the desired location for all of the cases considered using a roughness strip with  $k_R$  and the streamwise extent of the strip,  $\Delta s$ , given by the following correlations.

$$\frac{k_R}{\delta_t} = \max \left\{ \frac{5000}{\sqrt{Re_{s_t}}}, 3 \right\} \quad (5.3)$$

$$\frac{\Delta s}{\delta_t} = 0.015 \sqrt{Re_{s_t}} \quad (5.4)$$

The quantities  $\delta_t$  and  $Re_{s_t}$  are the boundary-layer thickness and transition Reynolds number based on arc length.

## 5.2 Applications

In order to test the new transition-triggering method, we have computed all of the two-dimensional transitional boundary layer cases considered by Singer, et

al.<sup>9</sup> Our applications also include a Mach 20 re-entry case. Table 5.1 summarizes the cases we have done.

Table 5.1: Transitional Boundary Layer Test Cases

Flow	Description	$\nabla p$	Data Source
1	Incompressible Flat Plate	None	Schubauer-Klebanoff <sup>19</sup>
2	Favorable $\nabla p$	Favorable	Blair-Werle <sup>20</sup>
3	Supersonic Cone Flow	None	Fisher-Dougherty <sup>21</sup>
3	Supersonic Cone Flow	None	Chen, et al. <sup>22</sup>
4	Freestream Turbulence	None	Schubauer-Skramstad <sup>23</sup>
4	Freestream Turbulence	None	Blair <sup>24</sup>
5	Prolate Spheroid	Favorable	Meier-Kreplin-Ming <sup>25</sup>
6	Concave Surface	None	Swearingen-Blackwelder <sup>26</sup>
6	Mach 20, 5° Cone	None	Howard <sup>27</sup>

In all cases, computation begins at the plate leading edge, and the turbulence kinetic energy is initially set to an extremely small value, viz.,  $10^{-15}U_\infty^2$ , throughout the boundary layer. This value is too small to trigger transition naturally. The initial  $\omega$  profile is given by the exact laminar-flow solution to the model equations.<sup>11</sup>

In addition to testing the transition triggering method described above, we have tested the effect of the cross-diffusion term in Equation (2.5). A disappointing feature of our previous transition predictions was a mild sensitivity of transition location to the initial  $\omega$  profile. The sensitivity was caused by the small, but noticeable, effect of the freestream value of  $\omega$  on the laminar-flow solution for  $\omega$ . The primary reason for introducing the cross-diffusion term was to eliminate this sensitivity for transition predictions. As shown in the preceding chapters, the cross-diffusion term eliminates most of the sensitivity for turbulent shear flows. Numerical experimentation for several of the transitional cases listed in Table 5.1 verifies that this is true for transitional flows also. That is, our computations verify that transition predictions are completely insensitive to the initial  $\omega$  profile, even when transition is triggered by freestream turbulence.

**Incompressible Flat Plate.** The first case is Flow 1 from Singer, et al.<sup>9</sup> This is an incompressible flat-plate boundary layer that undergoes transition at a plate length between 1.6 m. and 1.8 m. According to Equations (5.3) and (5.4), this flow requires a roughness strip with  $k_R/\delta_t = 3.0$  and  $\Delta s/\delta_t = 25$ . Numerical experimentation shows that a shorter transition strip, i.e.,  $\Delta s/\delta_t = 7$  is sufficient to trigger transition at the desired location for this case.

Figure 5.1 compares computed and measured skin friction throughout the transition region for the model with and without the cross-diffusion term. In both cases, computed and measured  $c_f$  differ by less than 16% of the peak skin

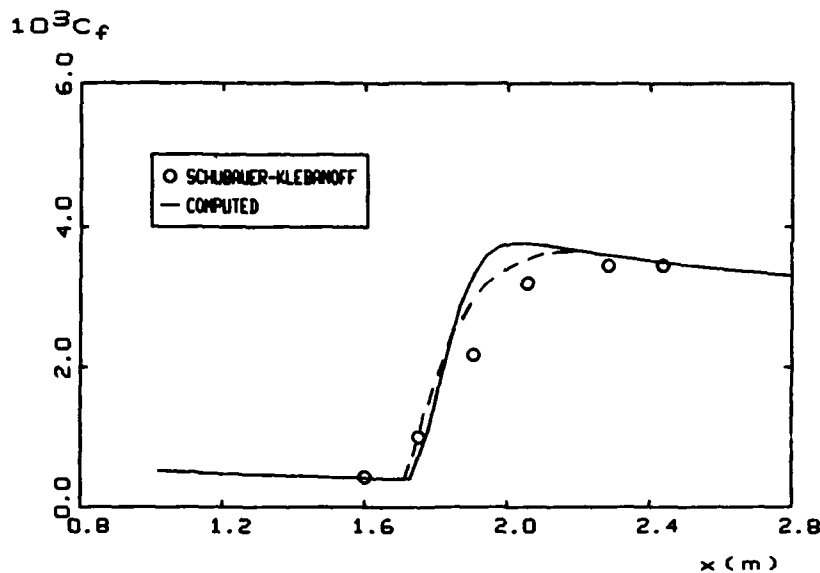
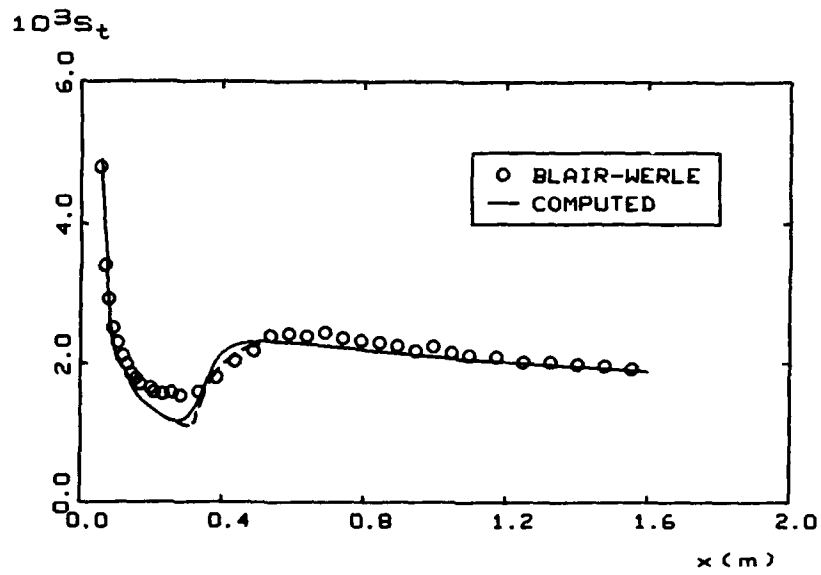


Figure 5.1: Transitional incompressible flat-plate boundary layer; — New  $k-\omega$  model; - -  $k-\omega$  model without cross diffusion.

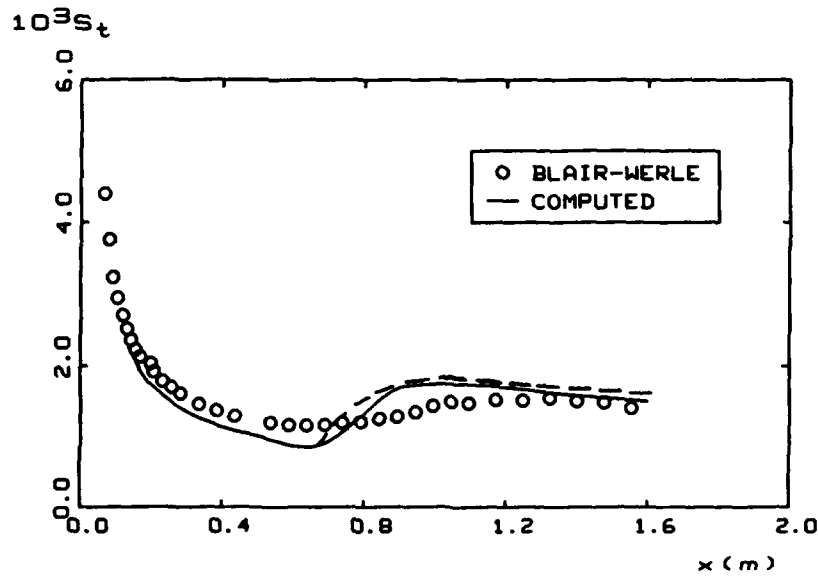
friction. Note that with cross-diffusion included, the distance between minimum and maximum skin friction is a bit less than that without cross diffusion.

**Favorable Pressure Gradient Boundary Layers.** The next applications are for incompressible boundary layers in a favorable pressure gradient. The boundary layers considered correspond to Flow 2/Cases 1 and 2 of Singer, et al. In addition to having adverse pressure gradient, the surface is cooled. Figure 5.2 compares computed and measured Stanton number for the two cases. Case 2 has a stronger favorable pressure gradient than Case 1. The dimensions of the roughness strip required to match the measured transition point are  $(k_R/\delta_l, \Delta s/\delta_l) = (10, 10)$  and  $(4, 9)$ , respectively, for Cases 1 and 2. Equations (5.3) and (5.4) indicate  $(k_R/\delta_l, \Delta s/\delta_l) = (8.5, 8.7)$  and  $(6.0, 12.5)$ , respectively. Again, we see that the transition width is reduced a bit when the cross-diffusion term is included.

**Supersonic Cone Flow.** For this application we consider Flow 3 of the Singer, et al. study. Cases 1-4 focus on flow past a  $5^\circ$  half angle cone with Mach numbers ranging from 1.16 to 1.86, corresponding to measurements of Fisher and Dougherty.<sup>21</sup> Cases 5-7 are for Mach 3.36 flow past a  $5^\circ$  half-angle cone, with an adiabatic surface (see Chen, et al.<sup>22</sup>). Table 5.2 summarizes the transition Reynolds number,  $Re_{x_t}$ , and Reynolds number based on transition width,  $Re_{\Delta x_t}$ , for all 7 cases, for the new and old low-Reynolds-number  $k-\omega$  models.



Case 1: Mildly favorable pressure gradient



Case 2: Strongly favorable pressure gradient

Figure 5.2: Transitional incompressible boundary-layer flow with favorable pressure gradient and surface cooling; — New  $k-\omega$  model; - - -  $k-\omega$  model without cross diffusion.

Table 5.2: Results for Fisher-Dougherty and Chen et al. Test Cases

Case	Mach Number	$Re_{x_t}$	$(Re_{\Delta x_t})_{new}$	$(Re_{\Delta x_t})_{old}$	$(Re_{\Delta x_t})_{exp}$
1	1.16	$7.13 \cdot 10^6$	$0.45 \cdot 10^6$	$0.89 \cdot 10^6$	$0.69 \cdot 10^6$
2	1.30	$5.70 \cdot 10^6$	$0.50 \cdot 10^6$	$0.84 \cdot 10^6$	$0.97 \cdot 10^6$
3	1.55	$7.90 \cdot 10^6$	$0.72 \cdot 10^6$	$1.08 \cdot 10^6$	$1.24 \cdot 10^6$
4	1.86	$7.49 \cdot 10^6$	$0.78 \cdot 10^6$	$1.07 \cdot 10^6$	$1.56 \cdot 10^6$
5	3.36	$6.92 \cdot 10^6$	$1.01 \cdot 10^6$	$1.63 \cdot 10^6$	---
6	3.36	$9.51 \cdot 10^6$	$1.19 \cdot 10^6$	$1.79 \cdot 10^6$	---
7	3.36	$1.07 \cdot 10^7$	$1.30 \cdot 10^6$	$1.82 \cdot 10^6$	---

**Freestream Turbulence Effects.** We turn now to effects of freestream turbulence, i.e., Flow 4 of the Singer, et al. study. All of the cases considered are for incompressible boundary layers. Table 5.3 shows that computed transition width for Cases 1-5 is consistently smaller than measured, and noticeably smaller than the model without cross diffusion.

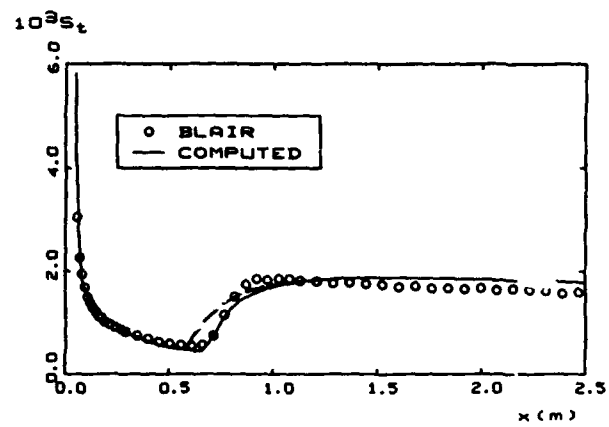
Table 5.3: Results for Schubauer-Skrainstad Test Cases

Case	$T'$	$Re_{x_t}$	$(Re_{\Delta x_t})_{new}$	$(Re_{\Delta x_t})_{old}$	$(Re_{\Delta x_t})_{exp}$
1	.042%	$2.85 \cdot 10^6$	$0.56 \cdot 10^6$	$0.88 \cdot 10^6$	$1.00 \cdot 10^6$
2	.100%	$2.75 \cdot 10^6$	$0.52 \cdot 10^6$	$0.86 \cdot 10^6$	$1.20 \cdot 10^6$
3	.200%	$2.20 \cdot 10^6$	$0.48 \cdot 10^6$	$0.78 \cdot 10^6$	$1.50 \cdot 10^6$
4	.260%	$1.80 \cdot 10^6$	$0.45 \cdot 10^6$	$0.69 \cdot 10^6$	$1.40 \cdot 10^6$
5	.340%	$1.40 \cdot 10^6$	$0.36 \cdot 10^6$	$0.58 \cdot 10^6$	$1.25 \cdot 10^6$

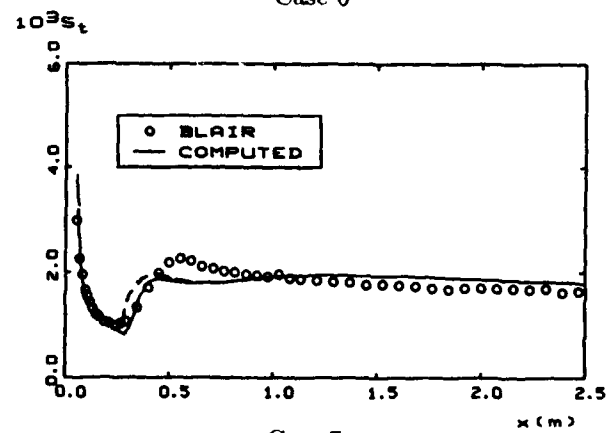
For Cases 6, 7 and 8, Figure 5.3 shows that predicted peak skin friction is about 10%-15% lower than measured. The results for these three cases are very similar to those obtained without cross diffusion.

**Incompressible Flow Past a Spheroid.** This case is Flow 5 from Singer, et al. The flow examines transition of a boundary layer over a prolate spheroid at zero angle of attack, with transition triggered by a roughness strip. Experimental data have been provided by Meier, Kreplin and Ming.<sup>25</sup> Table 5.4 summarizes the four cases.

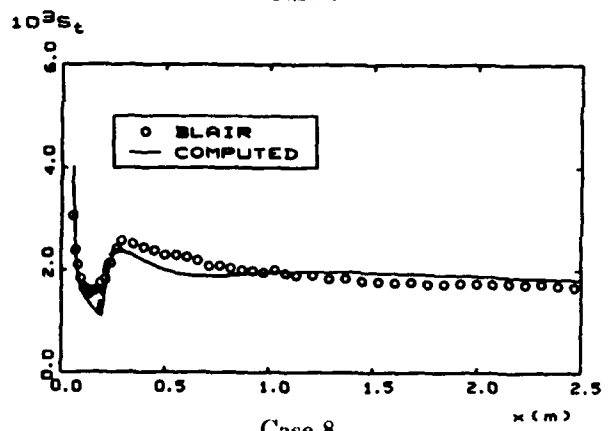
Figures 5.4 through 5.7 compare computed and measured skin friction (based on local boundary-layer edge velocity) as a function of arc length along the spheroid. As shown, computed and measured skin friction are closest when transition is induced by the roughness strip. Without the roughness strip, the predicted transition occurs more abruptly than measured.



Case 6



Case 7



Case 8

Figure 5.3: Transition width for flat-plate boundary layers; — New  $k-\omega$  model; - - -  $k-\omega$  model without cross diffusion.

Table 5.4: Meier-Kreplin-Ming Test Cases

Case	Description	$k_R/\delta_t$	$\Delta s/\delta_t$
1	$U_\infty = 20$ m/sec, no roughness strip	2.0	6.0
2	$U_\infty = 20$ m/sec, with roughness strip	4.0	8.0
3	$U_\infty = 30$ m/sec, no roughness strip	2.0	1.6
4	$U_\infty = 30$ m/sec, with roughness strip	2.0	15.0

**Concave Surface Boundary Layer.** In this application we consider incompressible flow over a concave surface. We present results in Figure 5.8. As in all previous applications, including cross diffusion causes a noticeable reduction in transition width. According to Equations (5.3) and (5.4), the transition strip should have  $k_R/\delta_t = 3.5$  and  $\Delta s/\delta_t = 21$ . Numerical experimentation shows that somewhat smaller values,  $k_R/\delta_t = 3.0$  and  $\Delta s/\delta_t = 12$ , can be used.

**Mach 20, 5° Cone.** Figure 5.9 compares computed and measured Stanton number,  $St$ , for Mach 20 flow<sup>27</sup> past a 5° half-angle cone. As shown, the computed Stanton number increases more abruptly than measured, although less abruptly with cross diffusion included. This is the only case for which transition width increases when cross diffusion is included. Note also, that the computed Stanton number downstream of transition is closer to measurements with cross diffusion included. Equations (5.3) and (5.4) indicate a transition strip with  $k_R/\delta_t = 3.0$  and  $\Delta s/\delta_t = 152$ . Numerical experimentation shows that transition can be triggered with  $k_R/\delta_t = 1.0$  and  $\Delta s/\delta_t = 32$ .

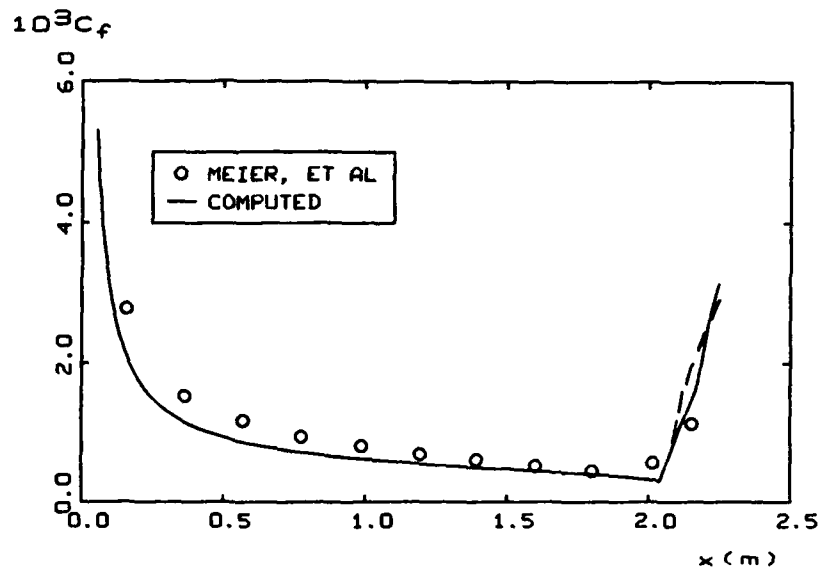


Figure 5.4: Flow past a prolate spheroid;  $U_\infty = 20$  m/sec; no roughness strip; — New  $k-\omega$  model; - - -  $k-\omega$  model without cross diffusion.

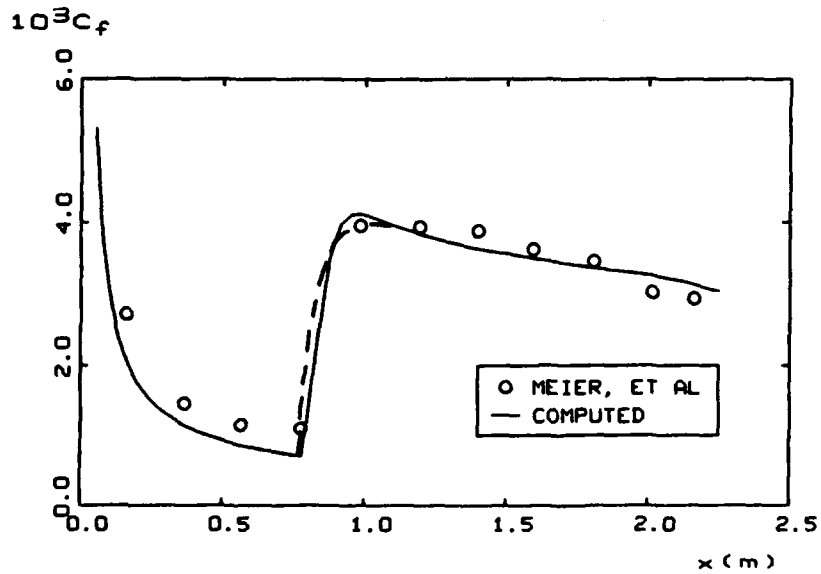


Figure 5.5: Flow past a prolate spheroid;  $U_\infty = 20$  m/sec; with roughness strip; — New  $k-\omega$  model; - - -  $k-\omega$  model without cross diffusion.

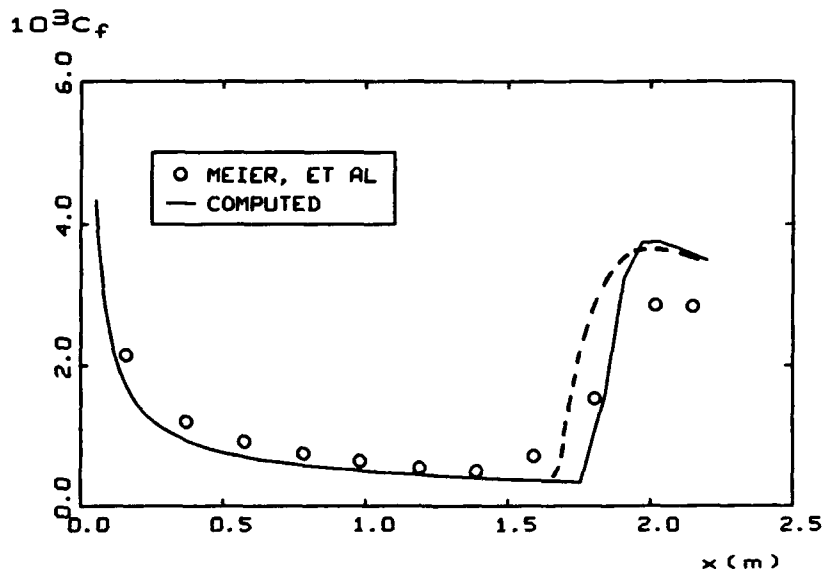


Figure 5.6: Flow past a prolate spheroid;  $U_\infty = 30$  m/sec; no roughness strip; — New  $k-\omega$  model; - - -  $k-\omega$  model without cross diffusion.

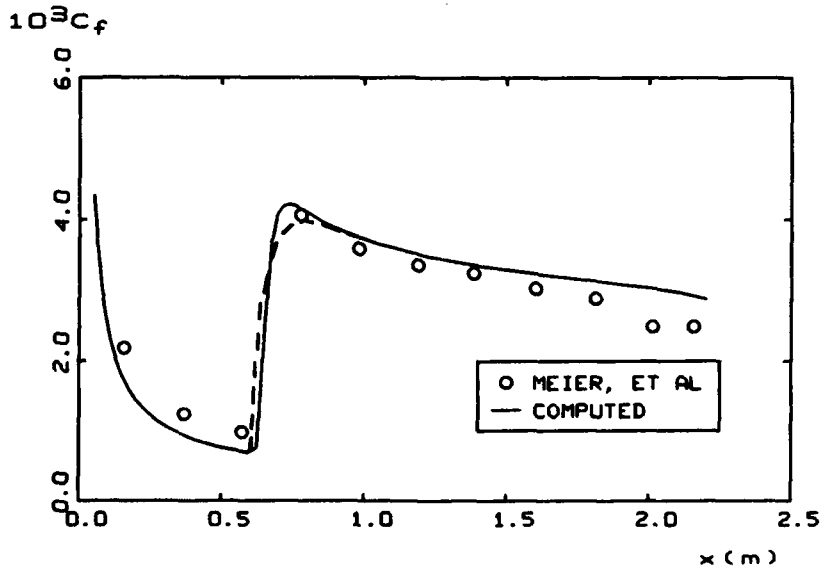


Figure 5.7: Flow past a prolate spheroid;  $U_\infty = 30$  m/sec; with roughness strip; — New  $k-\omega$  model; - - -  $k-\omega$  model without cross diffusion.

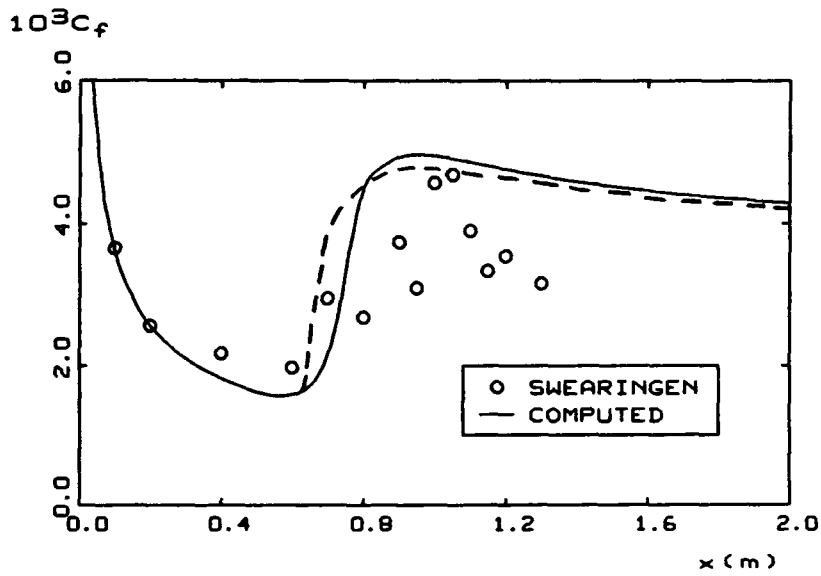


Figure 5.8: Transitional flow on a concave surface; incompressible flow; — New  $k-\omega$  model; ---  $k-\omega$  model without cross diffusion.

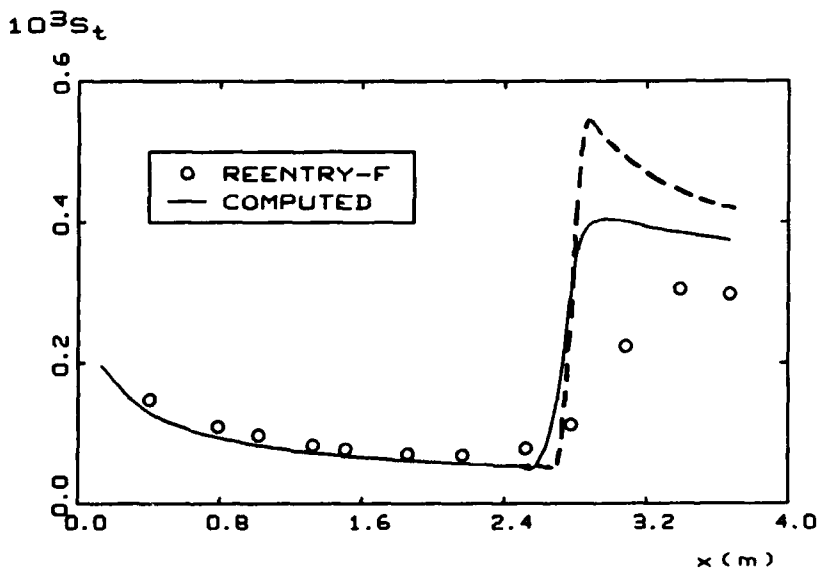


Figure 5.9: Mach 20 flow past a  $5^\circ$  half-angle cone; — New  $k-\omega$  model; ---  $k-\omega$  model without cross diffusion.

## Chapter 6

# Summary and Conclusions

In the context of turbulent boundary layers, this report shows that the new low-Reynolds-number version of the model retains most of the best features of the baseline, high-Reynolds-number version of the model. Most notably, the model is just as accurate as the baseline model for flows with adverse pressure gradient. This guarantees that the model approaches the correct post-transition, asymptotic state.

The cross-diffusion term is very effective in eliminating solution sensitivity to the freestream value of  $\omega$  for turbulent boundary layers, free shear flows and transitional boundary layers. However, this has been accomplished at the cost of a noticeable increase in the stiffness of the equations of motion.

While the new transition-triggering method has proved to be very effective, and the cross-diffusion term eliminates transition sensitivity to the initial  $\omega$  profile, computed transition width is actually reduced somewhat with cross diffusion included. Equation (5.3) is an upper bound for the roughness height required to trigger transition for all of the cases considered. In many cases, a smaller roughness height is sufficient, and the user should try different roughness heights, if possible, to determine the optimum height for a given application. Equation (5.4) is less certain. The formula also expresses an upper bound that covers all of the cases considered. The actual values used permits the roughness strip to persist for at least three streamwise finite-difference cells.

## Appendix A

# Compressible Law of the Wall

While the cross-diffusion term is very effective in eliminating the  $k$ - $\omega$  model's sensitivity to the freestream value of  $\omega$ , it has a negative impact on predictions for compressible boundary layers. Figure A.1 compares computed and measured velocity profiles for Mach 4.5 and Mach 10.3 flat-plate boundary layers. The computations have been done with all closure coefficients chosen to insure that the law of the wall holds in the limit of incompressible flow, viz,

$$u^+ = \frac{1}{\kappa} \ln y^+ + B \quad (\text{A.1})$$

with  $\kappa = 0.41$  and  $B = 5.0$ . As shown, when cross diffusion is omitted ( $\sigma_d = 0$ ), the law of the wall (in terms of Van Driest<sup>28</sup> variables) is reproduced, and close agreement with measured velocities is obtained. By contrast, when  $\sigma_d$  is 0.5 (with  $\sigma_d/\sigma = 1$ ), significant differences between computed and measured velocities appear at both Mach numbers. The figures indicate smaller differences for  $\sigma_d = 0.3$  (with  $\sigma_d/\sigma = 1/2$ ), and this is the value used in all computations of Chapters 3 through 5.

To explain the adverse effect of cross diffusion on the compressible law of the wall, this appendix examines  $k$ - $\omega$  model predicted compressible log-layer structure. The results are particularly illuminating and clearly demonstrate why using too large a ratio of  $\sigma_d$  to  $\sigma$  in the cross-diffusion term adversely affects compressible boundary-layer predictions. Aside from inclusion of the cross-diffusion term, the analysis is the same as that presented by Wilcox.<sup>29</sup>

The log layer is the region sufficiently close to the solid boundary for neglect of convective terms and far enough distant for molecular diffusion terms to be dropped. In the log layer, the equations of motion based on the  $k$ - $\omega$  model simplify to the following.

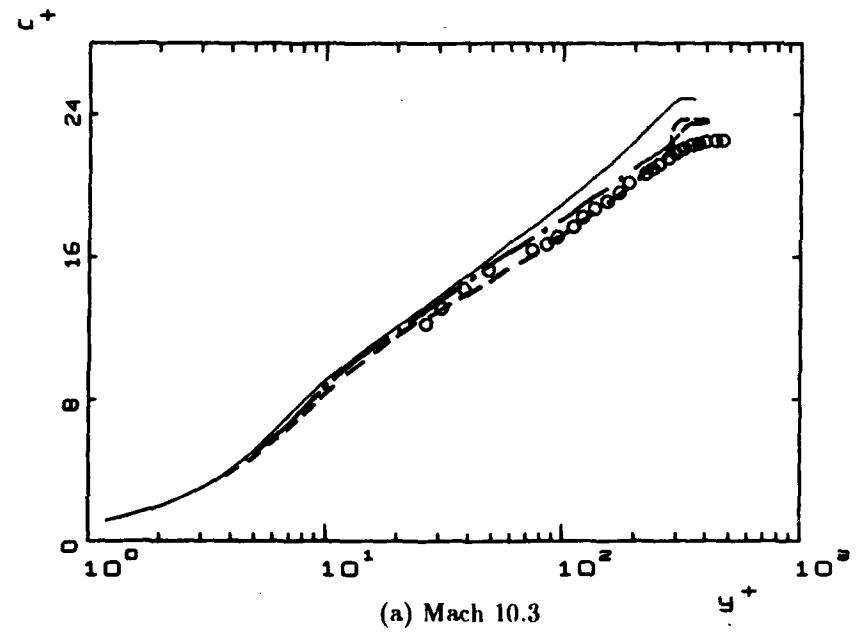
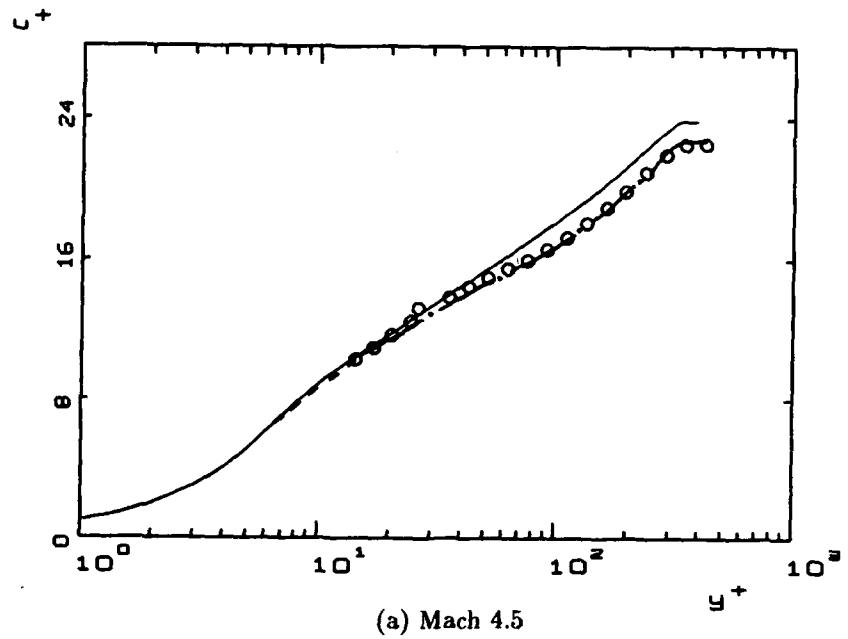


Figure A.1: Comparison of computed and measured velocity profiles for compressible flat-plate boundary layers; —  $\sigma_d = .5$ ; - - -  $\sigma_d = .3$ ; - - -  $\sigma_d = 0$ ;  $\circ$  Coles;  $\square$  Watson.

$$\mu_T \frac{du}{dy} = \rho_w u_\tau^2 \quad (\text{A.2})$$

$$\mu_T \frac{d}{dy} \left[ \frac{C_p T}{Pr_T} + \frac{1}{2} u^2 + \sigma^* k \right] = -q_w \quad (\text{A.3})$$

$$\sigma^* \frac{d}{dy} \left[ \mu_T \frac{dk}{dy} \right] + \mu_T \left( \frac{du}{dy} \right)^2 - \beta^* \rho \omega k = 0 \quad (\text{A.4})$$

$$\sigma \frac{d}{dy} \left[ \mu_T \frac{d\omega}{dy} \right] + \sigma_d \frac{\rho}{k} \frac{dk}{dy} \frac{d\omega}{dy} + \alpha \rho \left( \frac{du}{dy} \right)^2 - \beta \rho \omega^2 = 0 \quad (\text{A.5})$$

$$\rho T = \rho_w T_w \quad (\text{A.6})$$

The quantity  $u_\tau$  is friction velocity defined as  $\sqrt{\tau_w/\rho_w}$  where  $\tau_w$  is surface shear stress and  $\rho_w$  is density at the surface. Also,  $T_w$  is surface temperature,  $q_w$  is surface heat flux and  $C_p$  is specific heat at constant pressure. Finally,  $y$  is distance from the surface.

We now change independent variables from  $y$  to  $u$ . Consequently, derivatives transform according to

$$\mu_T \frac{d}{dy} = \mu_T \frac{du}{dy} \frac{d}{du} = \rho_w u_\tau^2 \frac{d}{du} \quad (\text{A.7})$$

With this change of dependent variables, we replace Equations (A.3)-(A.5) by the following.

$$\frac{d}{du} \left[ \frac{C_p T}{Pr_T} + \frac{1}{2} u^2 + \sigma^* k \right] = -\frac{q_w}{\rho_w u_\tau^2} \quad (\text{A.8})$$

$$\sigma^* \frac{d^2 k}{du^2} + 1 - \frac{\beta^* \rho^2 k^2}{\rho_w^2 u_\tau^4} = 0 \quad (\text{A.9})$$

$$\sigma \frac{d^2 \omega}{du^2} + \frac{\sigma_d}{k} \frac{dk}{du} \frac{d\omega}{du} + \alpha \frac{\omega}{k} - \frac{\beta \rho^2 k \omega}{\rho_w^2 u_\tau^4} = 0 \quad (\text{A.10})$$

Integrating Equation (A.8) yields the temperature, and hence the density, as a function of velocity and Mach number based on friction velocity,  $M_\tau \equiv u_\tau/a_w$ .

$$\frac{T}{T_w} = \frac{\rho_w}{\rho} = 1 - (\gamma - 1) Pr_T M_\tau^2 \left[ \frac{1}{2} \left( \frac{u}{u_\tau} \right)^2 + \frac{q_w}{\rho_w u_\tau^3} \left( \frac{u}{u_\tau} \right) + \sigma^* \left( \frac{k}{u_\tau^2} \right) \right] \quad (\text{A.11})$$

Next, we assume a solution of the form:

$$\rho k = \Gamma \rho_w u_\tau^2 \quad (\text{A.12})$$

where  $\Gamma$  is a constant to be determined. Substituting Equations (A.11) and (A.12) into Equation (A.9), and noting that  $M_t^2 = 2\Gamma M_\tau^2$ , leads to the following cubic equation for  $\Gamma$ .

$$\beta^* [1 + (\gamma - 1)Pr_T \sigma^* M_\tau^2 \Gamma] \Gamma^2 = 1 \quad (\text{A.13})$$

As can easily be verified, when  $M_\tau^2 \ll 1$ , the asymptotic solution for  $\Gamma$  is

$$\Gamma = \frac{1}{\sqrt{\beta^*}} - \left[ \frac{(\gamma - 1)Pr_T \sigma^*}{2\beta^*} \right] M_\tau^2 + \dots \quad (\text{A.14})$$

Finally, in terms of  $\Gamma$ , Equation (A.10) simplifies to

$$\sigma \frac{d^2 \omega}{du^2} - \frac{\sigma_d}{\rho} \frac{d\rho}{du} + [\alpha - \beta \Gamma^2] \frac{\rho \omega}{\rho_w u_\tau^2 \Gamma} = 0 \quad (\text{A.15})$$

Combining Equations (A.11) and (A.12) yields the density as a function of velocity and  $\Gamma$ .

$$\frac{\rho_w}{\rho} = \frac{1 - \frac{(\gamma-1)}{2} Pr_T M_\tau^2 \left[ \left( \frac{u}{u_\tau} \right)^2 + \frac{2q_w}{\rho_w u_\tau^3} \left( \frac{u}{u_\tau} \right) \right]}{1 + (\gamma - 1) Pr_T \sigma^* \Gamma M_\tau^2} \quad (\text{A.16})$$

Equation (A.16) assumes a more compact form if we introduce the freestream velocity,  $U_\infty$ . A bit more algebra yields

$$\frac{\rho_w}{\rho} = \frac{1 + Bv - A^2 v^2}{1 + (\gamma - 1) Pr_T \sigma^* \Gamma M_\tau^2} \quad (\text{A.17})$$

where

$$\left. \begin{aligned} v &= u/U_\infty \\ A^2 &= \frac{(\gamma-1)}{2} Pr_T M_\infty^2 (T_\infty/T_w) \\ B &= -Pr_T q_w U_\infty / (C_p T_w \tau_w) \end{aligned} \right\} \quad (\text{A.18})$$

Using Equations (A.14), (A.17) and (A.18), and retaining terms up to  $O(M_\tau^2)$ , Equation (A.15) assumes the following form,

$$\frac{d^2 \omega}{dv^2} + \frac{\sigma_d}{\sigma} \left[ \frac{B - 2A^2 v}{1 + Bv - A^2 v^2} \frac{d\omega}{dv} \right] - \left[ \frac{K_\omega^2 (U_\infty/u_\tau)^2}{1 + Bv - A^2 v^2} \right] \omega = 0 \quad (\text{A.19})$$

where the constant  $K_\omega$  is defined by

$$K_\omega^2 = \kappa^2 - \left[ \frac{(\gamma - 1) Pr_T (3\alpha - \beta/\beta^*) \sigma^*}{2\sigma} \right] M_\tau^2 + \dots \quad (\text{A.20})$$

and  $\kappa$  is Kármán's constant. Because  $U_\infty/u_\tau \gg 1$ , we can use the WKB method to solve Equation (A.19). Noting that  $\omega$  decreases as  $u/U_\infty$  increases, the asymptotic solution for  $\omega$  is

$$\omega \sim C [1 + Bv - A^2v^2]^{(1-2\sigma_d/\sigma)/4} \exp[-K_\omega u^*/u_\tau] \quad (\text{A.21})$$

where  $C$  is a constant of integration and  $u^*$  is defined by

$$\frac{u^*}{U_\infty} = \frac{1}{A} \sin^{-1} \left( \frac{2A^2v - B}{\sqrt{B^2 + 4A^2}} \right) \quad (\text{A.22})$$

Combining Equations (A.2), (A.12) and (A.21), we can relate velocity and distance from the surface.

$$\int [1 + Bv - A^2v^2]^{(2\sigma_d/\sigma-1)/4} \exp[K_\omega u^*/u_\tau] dv \sim \frac{Cy}{\Gamma U_\infty} \quad (\text{A.23})$$

We integrate by parts to generate the asymptotic expansion of the integral in Equation (A.23) as  $U_\infty/u_\tau \rightarrow \infty$ . Hence,

$$[1 + Bv - A^2v^2]^{(1+2\sigma_d/\sigma)/4} \exp[K_\omega u^*/u_\tau] \sim \frac{K_\omega Cy}{\Gamma u_\tau} \quad (\text{A.24})$$

Finally, we set the constant of integration  $C = \Gamma u_\tau^2 / (K_\omega \nu_w)$ . Taking the natural log of Equation (A.24), we conclude that

$$\frac{u^*}{u_\tau} \sim \frac{1}{K_\omega} \ln \left( \frac{u_\tau y}{\nu_w} \right) + B_\omega \quad (\text{A.25})$$

The quantity  $B_\omega$  is the effective "constant" in the law of the wall defined by

$$B_\omega = B + \frac{1}{K_\omega} \ln \left( \frac{\rho}{\rho_w} \right)^{(1+2\sigma_d/\sigma)/4} \quad (\text{A.26})$$

where  $B$  is a true constant.

As discussed by Willcox,<sup>29</sup> the difference between  $K_\omega$  and the Kármán constant is of no great consequence. However, the variation of  $B_\omega$  with the density ratio has a large effect on both skin friction and the predicted law of the wall. As clearly demonstrated by Wilcox,<sup>13</sup> the magnitude of the power to which  $\rho/\rho_w$  is raised determines the degree of distortion of the velocity profile. For example, the Standard  $k-\epsilon$  model is equivalent to a  $k-\omega$  model with  $\sigma_d = 2\sigma$ . This corresponds to an exponent of 5/4, while the unmodified  $k-\omega$  model has an exponent of 1/4. As shown in Figure A.1, there is virtually no distortion of the compressible law of the wall when  $\sigma_d = 0$ . By contrast, for the  $\sigma_d = 0.3$  and  $\sigma_d = 0.5$  cases we have used  $\sigma = 0.6$  and  $\sigma = 0.5$ , respectively, so that the corresponding exponents are 1/2 and 3/4, respectively. The figure shows increasing distortion of the compressible law of the wall as  $\sigma_d$  increases. Although

not shown, the  $k-\epsilon$  model departs even farther from the compressible law of the wall.

As a final comment, if we had written the cross-diffusion term as

$$\text{Cross diffusion} = \frac{\sigma_d}{\omega} \frac{\partial(\rho k)}{\partial x_j} \frac{\partial \omega}{\partial x_j} \quad (\text{A.27})$$

the exponent in Equation (A.26) would be reduced to  $1/4$ , independent of the value of  $\sigma_d$ . This is true only for the constant-pressure case since  $\rho k$  is approximately constant in the log layer. The same statement cannot be made for boundary layers with nonzero pressure gradient, however. A shortage of Contract funds precluded testing this alternative.

## References

1. Wilcox, D. C. "Reassessment of the Scale Determining Equation for Advanced Turbulence Models," *AIAA Journal*, Vol. 26, No. 11, pp. 1299-1310 (1988).
2. Wilcox, D. C., "Turbulence-Model Transition Predictions," *AIAA Journal*, Vol. 13, No. 2, pp. 241-243 (1975).
3. Wilcox, D. C., "Turbulence Model Transition Predictions: Effects of Surface Roughness and Pressure Gradient," AIAA Paper 75-857 (1975).
4. Wilcox, D. C. and Chambers, T. L., "Application of the Turbulence-Model Transition-Prediction Method to Flight Test Vehicles," *Turbulence in Internal Flows*, S. N. B. Murthy, pp. 233-247 (1976).
5. Wilcox, D. C., "A Model for Transitional Flows," AIAA Paper 77-126 (January 1977).
6. Wilcox, D. C., "Alternative to the  $e^9$  Procedure for Predicting Boundary-Layer Transition," *AIAA Journal*, Vol. 19, No. 1, pp. 56-64 (January 1981).
7. Wilcox, D. C. and Marvin, J. G., "Combined Effects of Freestream Turbulence and Mass Addition on Blunt-Body Heating and Transition," Proceedings of the 2<sup>nd</sup> ASME/JSME Joint Thermal Engineering Conference, Honolulu, Hawaii (March 1987).
8. Mansour, N. N., Kim, J. and Moin, P., "Reynolds Stress and Dissipation Rate Budgets in Turbulent Channel Flow," *Journal of Fluid Mechanics*, Vol. 194, pp. 15-44 (1988).
9. Singer, B. A., Dinavahi, S. P. G. and Iyer, V., "Testing of Transition-Region Models: Test Cases and Data," NASA CR 4371 (May 1991).
10. Favre, A., "Equations des Gaz Turbulents Compressibles," *J. Mecan.*, Vol. 4, No. 3, pp. 361-390 (1965).

11. Wilcox, D. C., "The Remarkable Ability of Turbulence Model Equations to Describe Transition," Fifth Symposium on Numerical and Physical Aspects of Aerodynamic Flows, California State Univ., Long Beach, California (13-15 January 1992).
12. Menter, F. R. "Improved Two-Equation  $k-\omega$  Turbulence Models for Aerodynamic Flows," NASA TM-103975 (1992).
13. Wilcox, D. C., *Turbulence Modeling for CFD*, DCW Industries, Inc., La Cañada, CA (1992).
14. Wieghardt, K. and Tillman, W., "On the Turbulent Friction Layer for Rising Pressure," NACA TM 1314 (1951).
15. Samuel, A. E. and Joubert, P. N., "A Boundary Layer Developing in an Increasingly Adverse Pressure Gradient," *Journal of Fluid Mechanics*, Vol. 66, p. 481 (1975).
16. Fernholz, H. H. and Finley, P. J., "A Critical Compilation of Compressible Turbulent Boundary Layer Data," AGARDograph No. 223 (1977).
17. Kline, S. J., Cantwell, B. J. and Lilley, G. M., *1980-81 AFOSR-HTTM-Stanford Conference on Complex Turbulent Flows*, Stanford Univ., CA (1981).
18. Wilcox, D. C., "Application of Low Reynolds Number Two-Equation Turbulence Models to High Reynolds Number Flows," International Conference on Near-Wall Turbulent Flows, Arizona State Univ., Tempe, AZ (March 15-17, 1993).
19. Schubauer, G. B. and Klebanoff, P. S., "Contributions on the Mechanics of Boundary-Layer Transition," NASA TN 3489 (1955).
20. Blair, M. F. and Werle, M. J., "Combined Influence of Free-Stream Turbulence and Favorable Pressure Gradients on Boundary Layer Transition and Heat Transfer," United Technologies Report No. R81-914388-17 (1981).
21. Fisher, D. F. and Dougherty, N. S., "Transition Measurements on a  $10^\circ$  Cone at Mach Numbers from 0.5 to 2.0," NASA TP-1971 (1982).
22. Chen, F.-J., Malik, M. R. and Beckwith, I. E., "Boundary-Layer Transition on a Cone and Flat Plate at Mach 3.5," *AIAA Journal*, Vol. 27, pp. 687-693 (1989).
23. Schubauer, G. B. and Skramstad, H. K., "Laminar-Boundary-Layer Oscillations and Transition on a Flat Plate," NACA Report No. 909 (1948).

24. Blair, M. F., "Influence of Free-Stream Turbulence on Boundary Layer Heat Transfer and Mean Profile Development, Part 1 - Experimental Data," *Transactions of the ASME, Journal of Heat Transfer*, Vol. 105, pp. 33-40 (1983).
25. Meier, H. L., Kreplin, H. P. and Ming, X., "Problems Associated with Artificial Boundary Layer Transition," AIAA Paper 83-1673 (1983).
26. Swearingen, J. D. and Blackwelder, R. F., "The Growth and Breakdown of Streamwise Vortices in the Presence of a Wall," *Journal of Fluid Mechanics*, Vol. 182, pp. 255-290 (1987).
27. Howard, F., "Thermal Analysis Methods and Basic Heat-Transfer Data for a Turbulent Heating Flight Experiment at Mach 20 (Re-entry F)," NASA TM X-2282 (1971).
28. Van Driest, E. R., "Turbulent Boundary Layer in Compressible Fluids," *Journal of the Aeronautical Sciences*, Vol. 18, pp. 145-160, 216 (1951).
29. Wilcox, D. C., "Dilatation-Dissipation Corrections for Advanced Turbulence Models," *AIAA Journal*, Vol. 30, No. 11, pp. 2639-2646 (1992).